Int. J. Heat Mass Transfer. Vol. 31, No. 10, pp. 2137–2145, 1988
Printed in Great Britain

0017–9310/88 $3.00 + 0.00

Buoyancy effects on laminar impinging jets

T. D. YUAN, J. A. LIBURDY and T. WANG
Department of Mechanical Engineering, Clemson University, Clemson, SC 29634, U.S.A.

(*Received* 23 *October* 1987 *and in final form* 28 *March* 1988)

Abstract—A laminar, heated, two-dimensional jet impinging on an isothermal surface has been studied to determine the effects of buoyancy on the flow and thermal structure of the region near impingement. The parameters used include the jet exit Reynolds number, Richardson number, and separation distance between the impinging surface and the jet exit. Results of the velocity profile, temperature distribution, local friction factor, and heat transfer coefficient are presented for both upward and downward facing jets. It is found that the local Nusselt number experiences a peak away from the axis of the jet which is enhanced for highly buoyant flows. In general, the enhancement of the heat transfer rate is substantial for high Richardson number conditions.

INTRODUCTION

IMPINGING heated jet flows occur in many industrial applications such as drying of textiles, paper, films, etc., and thermal treatment of materials. In some circumstances drying rates may be increased by an order of magnitude compared to contact drying. Numerous experimental and analytical studies have been reported on impinging jets. Despite the concern and attention to the problem there is a lack of understanding of the details of the heat transfer process. In an attempt to better understand the influence of several important parameters (i.e. flow geometry, orientation and jet heating) we have numerically studied a heated laminar two-dimensional jet. Our results concentrate primarily on the effects of buoyancy to augment the local heat transfer from an impinging jet to a fixed surface. Although laminar jets have limited applications, the results from this study are useful in understanding the impact of buoyancy on the flow structure and transport processes. These concepts can be extended to aid in the understanding of turbulent impinging jets.

Overall, laminar impinging jets have received relatively little attention in the literature. Analytically this problem has been solved using various assumptions. Enrich [1] first solved the potential flow problem for a jet with a uniform velocity profile at the nozzle exit which impinges on a flat plate by neglecting the effect of diffusion terms. Miyazaki and Silberman [2] used Enrich's potential flow solution to obtain free stream boundary conditions for the boundary layer equations that describe the flow close to the plate. The local skin friction and heat transfer along the plate were obtained for various nozzle to plate spacings. Sparrow and Lee [3] defined a criterion for neglecting the diffusion term for flat or parabolic velocity exit profiles.

Experimental work on this problem has primarily focused on local heat transfer measurements. Gardon and Akfirat [4] measured the local heat transfer rates for Reynolds numbers ranging from 450 to 22 000. However, from their measurements the initial velocity profiles were neither flat nor parabolic. Sparrow and Wong [5] measured the impingement heat transfer coefficient for an initially laminar fully developed slot jet using an analogy to naphthalene sublimation.

Numerical studies have mostly addressed the heated non-buoyant case. Wolfshtein [6] predicted the flow and temperature fields of turbulent and laminar impinging jets. In his analysis the problem domain is divided into a free jet region and an impinging region. The velocity profile at the end of the free jet region is used as a boundary condition for the impinging region. The results are limited to the case of a fully developed velocity profile at the jet exit. van Heiningen *et al.* [7] used the vorticity–stream function method to calculate the flow field and heat transfer of an impinging laminar slot jet and studied the effect of Reynolds number and initial jet velocity profile. However, for a large separation distance between the jet exit and the surface and for large Reynolds numbers, they were not able to obtain converged solutions. Mujumdar *et al.* [8] developed a numerical model to study a round laminar jet impinging normally onto a plane wall maintained at a constant wet-bulb temperature.

Mikhail *et al.* [9] numerically solved the flow field and heat transfer from a row of slot jets impinging on an isothermal flat plate. They found that the flow rate entrained into a flow field would not, in general, satisfy the overall mass balance. They proposed a mass imbalance equation to calculate the pressure correction along the free boundary from the overall mass conservation principle.

To the authors' knowledge, there is no reported work in the literature of buoyancy effects on laminar impinging jets. However, various studies of buoyancy effects in somewhat similar situations have been reported. Satyanarayana and Jaluria [10] found that

NOMENCLATURE

C_f	wall friction factor
C_f^*	$C_f \frac{1}{2}\sqrt{Re}$
g	acceleration of gravity
Gr	Grashof number, $g\beta(T_j - T_w)L^3/\nu^2$
h	local heat transfer coefficient by convection, $q/(T_j - T_w)$
H	slot height from the surface
H^*	non-dimensional slot height, H/L
k	thermal conductivity
L	half width of the slot
Nu	Nusselt number, hL/k
p	pressure
P	non-dimensional pressure, $(p - p_\infty)/\rho v_j^2$
Re	Reynolds number, $v_j L/\nu$
Ri	Richardson number, Gr/Re^2
S	source term
T	thermodynamic temperature
u	velocity component in the x-direction
U	non-dimensional velocity component in the x-direction, u/v_j
v	velocity component in the y-direction
V	non-dimensional velocity component in the y-direction, v/v_j
x	coordinate along the impinging surface from the stagnation point
X	non-dimensional coordinate, x/L
y	coordinate normal to the surface
Y	non-dimensional coordinate, y/L.

Greek symbols

α	thermal diffusivity
β	thermal expansion coefficient
Γ	diffusion coefficient
θ	non-dimensional temperature, $(T - T_w)/(T_j - T_w)$
μ	dynamic viscosity
ν	kinematic viscosity
ρ	density
τ	shear stress
ϕ	variable.

Subscripts

j	slot exit
m	maximum value of the variable
w	impinging surface
∞	ambient.

when a heated fluid is discharged at a downward inclination in a laminar slot jet the jet will eventually have a flow reversal if the exit buoyancy is sufficiently large. The downward penetration of the jet is found to increase with increasing flow inclination, with decreasing jet exit buoyancy and with increasing flow rate. Penetration was found to depend on the mixed convection parameter, the Richardson number, based on the jet exit conditions. Their analytical model agrees very well with experimental results. Another related study is the buoyancy effects on flow over a flat plate. Chen *et al.* [11] found that buoyancy introduces a longitudinal pressure gradient which modifies the flow. In their analysis, buoyancy is found to accelerate or decelerate the flow for a heated flow above or below a cooler surface, respectively. Mori [12] analytically predicted the effects of buoyancy for laminar flow over a horizontal surface. In each case of induced decelerating flow there is an upper limit of the mixed convection parameter beyond which flow will reverse. His results show that the local wall friction coefficient increases sharply in response to a favorable induced pressure gradient. For the adverse induced pressure gradient, due to negative buoyancy, the skin friction drops sharply. It is to be expected that the strength of adverse longitudinal pressure gradient will ultimately prompt flow separation. In the study of the buoyancy effects on forced laminar convection flow, the effects on transition and the nature of secondary flows were indicated to be closely linked.

None of the above-mentioned studies address the effects of buoyancy on the local wall friction and heat transfer of an impinging jet. Our results show the relative importance of buoyancy on the flow structure, the streamwise variation of the flow energy and the surface transport characteristics. The parameters which influence the results are the jet exit Reynolds number and Grashof number, and the surface position relative to the jet exit. Results are presented for a range of these parameters which are appropriate for a laminar impinging air jet.

ANALYSIS

The flow is considered to be two-dimensional, steady, incompressible, and laminar. The impinging surface is normal to the jet exit velocity and is isothermal. The jet exits through a slot of width $2L$ and is a distance H from the surface. The initial velocity and temperature profiles are assumed to be uniform and the ambient fluid is cooler than the jet fluid and is quiescent and isothermal. For large temperature differences between the exit jet flow and ambient, the effects of variations of physical properties may be important. The effects of viscosity and thermal conductivity can be discussed independently of buoyancy because buoyancy is not explicitly influenced by the variation of viscosity or of thermal conductivity. It is assumed that the density variation is only included to the extent that it contributes to the buoyancy force. The energy equation is formulated by neglecting the

Table 1. Boundary conditions

Boundary	Velocity	Temperature	Comment
I	$U=0$ $V=0$	$\theta=1$	Slot exit
II	$\partial U/\partial Y=0$ $\partial V/\partial Y=0$	$\partial\theta/\partial y=0$	Free surface
III	$U=0$ $\partial V/\partial X=0$	$\partial\theta/\partial X=0$	Axis of symmetry
IV	$\partial U/\partial X=0$ $\partial V/\partial X=0$	$\partial\theta/\partial X=0$	Outflow
V	$U=0$ $V=0$	$\theta=0$	Impingement
VI	$U=0$	$\theta=0$	Slot surface

viscous dissipation and the change of temperature due to compression.

Under these foregoing assumptions, the governing conservation equations of mass, momentum in the x- and y-directions and energy are

$$\partial u/\partial x+\partial v/\partial y=0 \tag{1}$$

$$\rho u\partial u/\partial x+\rho v\partial u/\partial y=-\partial p/\partial x+\mu(\partial^2 u/\partial x^2+\partial^2 u/\partial y^2) \tag{2}$$

$$\rho u\partial v/\partial x+\rho v\partial v/\partial y=-\partial p/\partial y+\mu(\partial^2 v/\partial x^2+\partial^2 v/\partial y^2)+\rho g \tag{3}$$

$$u\partial T/\partial x+v\partial T/\partial y=\alpha(\partial^2 T/\partial x^2+\partial^2 T/\partial y^2). \tag{4}$$

For relatively small changes of density with temperature, the body force term in equation (3) can be expressed in terms of the ambient conditions as

$$\rho g=\rho_\infty g+\rho g\beta(T_\infty-T). \tag{5}$$

The scaling parameters are chosen as v_j, the average velocity at the jet exit, L, the half width of the jet, T_j-T_w, the temperature difference between the jet exit and the surface, and ρv_j^2, the characteristic pressure. Non-dimensional variables are defined in the Nomenclature and are used to rewrite the governing equations as

$$\partial U/\partial X+\partial V/\partial Y=0 \tag{6}$$

$$U\partial U/\partial X+V\partial U/\partial Y=-\partial P/\partial X+1/Re(\partial^2 U/\partial X^2+\partial^2 U/\partial Y^2) \tag{7}$$

$$U\partial V/\partial X+V\partial V/\partial Y=-\partial P/\partial Y+1/Re(\partial^2 V/\partial X^2+\partial^2 V/\partial Y^2)+Ri\theta \tag{8}$$

$$U\partial T/\partial X+V\partial T/\partial Y=1/Re\,Pr(\partial^2 T/\partial X^2+\partial^2 T/\partial Y^2) \tag{9}$$

where the non-dimensional parameters Re, Ri, and Pr are also defined in the Nomenclature. The boundary conditions in non-dimensional form are given in Table 1 and are discussed with the solution procedure.

Solution procedure

The flow field is subdivided into finite volumes, each of which encloses an imaginary grid node. Scalar variables such as pressure, density, viscosity and temperature are evaluated at the grid node, while the velocity components are chosen to lie on the control volume faces where they are used for the mass flow rate computations. The set of governing differential equations are integrated to yield a set of finite difference equations. These finite difference equations are then solved together with a pressure correction equation to satisfy the continuity equation. The solution procedures follow that given by Patankar [13] in the program SIMPLE with a modification recommended by van Doormaal and Raithby [14].

In the development of the numerical simulation the specification of the boundary conditions requires very careful examination. Since primitive variables in the governing equations are used, the boundary conditions can be examined through their physical interpretation.

Because of symmetry it suffices to consider only one half of the flow field as shown in Fig. 1. The specification of boundary conditions I, III and V can be realized based on uniform velocity and temperature profiles, symmetry, no slip, and an isothermal surface. The slot surface, boundary VI, is located at the control volume surface and the values for v and T adjacent to the wall are obtained by linear interpolation.

The velocity at boundary II will not, in general, satisfy the overall mass balance. This mass imbalance can be significantly reduced by requiring the cal-

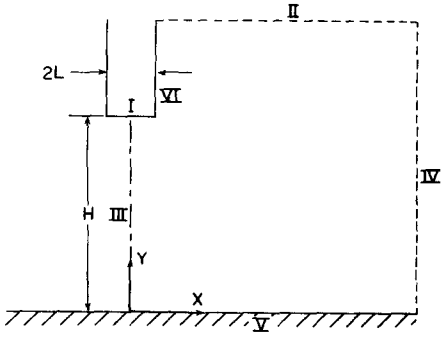

FIG. 1. Computational domain and identification of boundaries.

culation domain to be enlarged in both boundaries II and IV. When this boundary is expanded it accounts for both inward and outward flow conditions. As shown in the results the direction of the entrained flows at this boundary depends on the level of buoyancy. The specification of the boundary conditions at II has been tested for various situations. In this problem the surrounding fluid is assumed to be entrained into the flow such that the gradients of both velocity components and temperature gradients are negligible at boundary II. At the outflow boundary IV, the velocity and temperature variations in the X-direction are assumed to be negligible. This condition can only be fulfilled by using a properly expanded domain. Alternative boundary conditions at II and IV can be specified by requiring a mass balance with a smaller domain and less calculation time to achieve converged results. However, when this was tried the velocity profiles were unrealistic and indicated an ill-defined problem. Thus we selected the most realistic boundary condition with the price of a larger grid domain and subsequently longer calculation time for each iteration.

Numerical procedure

The governing equations are cast in the common form

$$\partial(\rho u_i \phi)/\partial x_i = \partial(\Gamma \partial\phi/\partial x_i)/\partial x_i + S. \qquad (10)$$

The first and second terms are convection and diffusion, respectively. The last term, S, is the mechanism for generation (or destruction) of ϕ. Whatever cannot be expressed through convection and diffusion terms can be combined into this source term as shown in Table 2 for each of the governing equations. Most of the results presented in this study were obtained using a non-uniform expanding 30 by 31 grid with grid elements closely spaced in regions of strong gradients of ϕ, namely along the surface and near the jet centerline.

Through numerical experiments it has been found that grid spacing, domain size and the flow parameters all contribute to obtaining grid independent solutions. The size of the domain is determined by the proper specification of the flow boundary especially in the free surface and outflow boundaries. The domain was, depending on the flow situations, increased to the necessary size by examining the velocity profile and pressure coefficient near the boundaries so that the boundary conditions were satisfied. The grid spacing of the domain was set by the coarsest possible grid which yielded less than 1% variation of the results at all grid points.

Table 2. Variables for the general equation

Equation	ϕ	Γ	Source
x-Momentum	U	$1/Re$	$-\partial P/\partial X$
y-Momentum	V	$1/Re$	$-\partial P/\partial Y + Gr\,\theta/Re^2$
Energy	θ	$1/Re\,Pr$	—

Table 3. Ranges of governing parameters

Re	Gr	Ri	Pr	H^*
10–500	10–125 000	−3 to 1.5	0.7	2–8

The ranges of flow parameters used in this study are given in Table 3. These parameters also affect the grid specification mentioned above. The size of the domain and the grid spacing required for each flow pattern have been investigated. For $H^* < 3$ the grid independent solutions are obtained for a total solution domain of $x_{max} = 12H$, $y_{max} = 6H$ and grid spacing of 30 by 24. At H^* greater than 3 and less than 8, the domain is $x_{max} = 15H$, $y_{max} = 8H$ and grid spacing of 30 by 31. In general, at higher values of H^*, Re and Ri, a larger computational domain and finer grid spacing was required. Thus the above limits represent a minimum for the grid independent solutions and were increased as needed. The calculation times for each case range from 2 min 30 s for the 30 by 24 case with 150 iterations and 5 min 40 s for the 30 by 31 case with 200 iterations using an NAS AS/XL-60.

The computational scheme was validated against the exact solution of two-dimensional stagnation flow [15]. In these calculations the free boundary conditions were also tested. The agreement is excellent.

RESULTS

Results are presented for both upward and downward facing jet flows impinging on a surface the temperature of which is equal to that of the ambient. The ranges of parameters chosen in this study are shown in Table 3. The upper limit of 500 for Re is based on that suggested by Gauntner *et al.* [16] for laminar flow. For Reynolds numbers below 150 McNaughton and Sinclair [17] defined the flow as a dissipated laminar jet in which the large viscous forces cause rapid diffusion of the jet into the surrounding fluid. The range of Grashof numbers studied is based on the limits for Re and the ability to obtain converged solutions. The limits of Gr and Re result in the Richardson number range indicated. Note that negative values of Richardson numbers are for upward facing, buoyancy assisted, flows and positive values are for downward, buoyancy retarded, flows. The values of H^* were kept small to be consistent with laminar flow. Not all of the results for all of the values of H^* are presented but the trends are identified. In this study it was found that numerical oscillations and divergence of the results occur for values of H^*, Re, and Ri beyond those reported.

The velocity and temperature distributions were determined for each set of conditions investigated. The distributions for three of the sets of conditions are shown in Fig. 2 for $H^* = 3$. For low Richardson and relatively high Reynolds numbers, Figs. 2(a) and

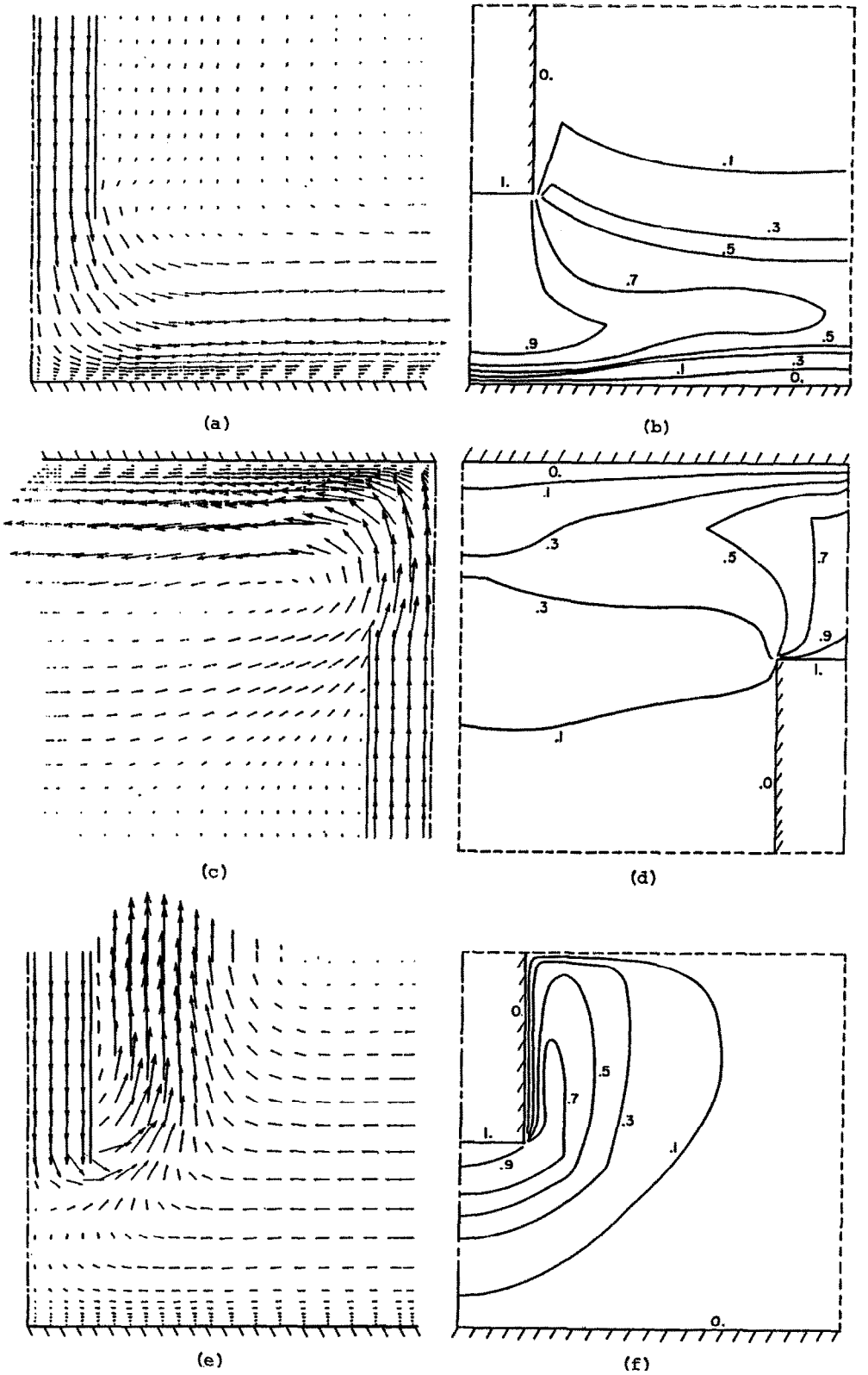

FIG. 2. Velocity and temperature distributions for: (a) and (b) $Re = 50$, $Ri = 0.1$, $H^* = 3$; (c) and (d) $Re = 10$, $Ri = -0.3$, $H^* = 3$; (e) and (f) $Re = 10$, $Ri = 1.5$, $H^* = 3$.

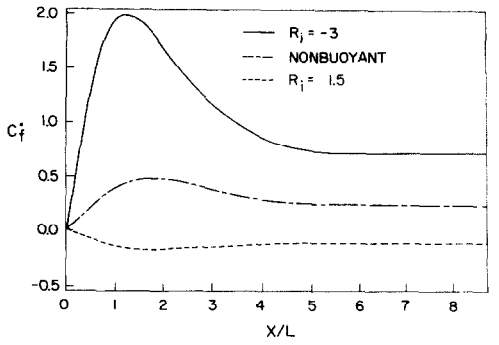

FIG. 3. Distribution of C_f^* along the impinging surface for $Re = 10$, $H^* = 3$ and large Ri.

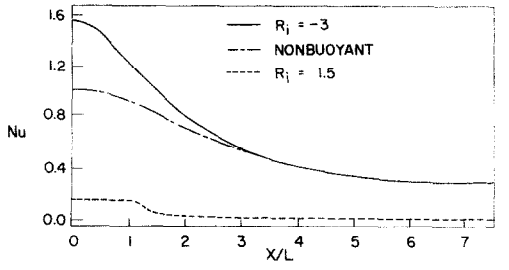

FIG. 4. Distribution of Nu along the impinging surface for $Re = 10$, $H^* = 3$ and large Ri.

(b), the flow and temperature distributions are very similar to the non-buoyant case and thus are not affected by direction. As the Richardson number increases the buoyancy forces become important, and as the effects of the initial jet momentum decays the flow becomes dominated by buoyancy. For the upward facing jet, Figs. 2(c) and (d), large values of Ri strengthen the flow with an increase in the inward or entrained flow just downstream of the jet exit. This results in lower jet temperatures as can be seen by comparing the temperature profiles of Figs. 2(b) and (d). The flow itself is strengthened by the buoyancy forces which, we show later, results in an enhanced wall friction and heat transfer.

For the case of a downward facing jet the buoyancy forces work against the flow. For large Richardson numbers the impinging velocity is reduced as is the wall friction and heat transfer rate. If the Richardson number is sufficiently large and negative the flow in the wall jet region eventually separates from the surface. In this situation ambient fluid is entrained in the reverse direction along the outer regions of the surface. For very large positive Richardson numbers the jet does not impinge on the surface and ambient fluid is drawn inward along the entire surface as shown in Fig. 2(e). When the absolute value of Ri is sufficiently small, both C_f and Nu are only slightly enhanced for the upward facing jet and slightly reduced for the downward facing jets, with the maximum values most affected. Details of these results are not presented.

The effects of large Richardson numbers on the local values of C_f and Nu are presented for $Re = 10$ and $H^* = 3$ in Figs. 3 and 4. In the upward facing case (negative Ri) there is a very strong enhancement of both C_f and Nu caused by the strengthening of the flow prior to impingement. Negative values of C_f occur for positive Richardson numbers. The sign change indicates the condition of flow reversal.

As an indication of the buoyancy effects on the friction coefficient and heat transfer coefficient the maximum values of C_f^* and Nu, for $Re = 30$, are shown in Figs. 5 and 6 vs Richardson number. Results are presented for $H^* = 3$, 6 and 8 and cover a wide range of buoyancy assisted and retarded flows. For the assisted flows there is a nearly linear decrease of C_f^* with increasing Ri. The rate of decrease is larger for larger H^* indicating that the increased development length provides greater buoyant interaction. The increase in the heat transfer coefficient follows the same trend. At a sufficiently large Ri there is a rapid decline of both C_f^* and Nu. This result can be linked to a drastic change in the flow field. As the buoyancy forces begin to dominate the downward facing flows the flow is retarded. The momentum at impingement is correspondingly reduced which decreases the surface transport characteristics.

The near impingement region was examined in detail to determine the buoyancy effects on the transport coefficients. In particular, it is desired to understand the relative impact of the exit Reynolds number and Richardson number on the transport process at the impinging surface. The Nusselt number distribution near impingement is shown in Fig. 7 for three values of Re and Ri for $H^* = 3$. Both buoyancy

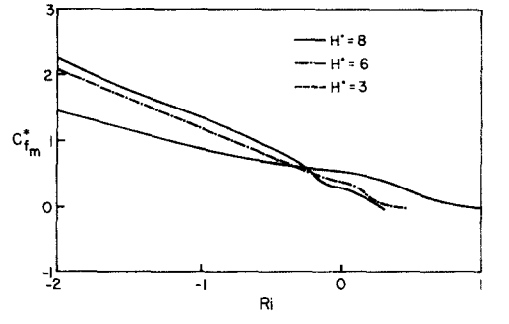

FIG. 5. The maximum value of the friction coefficient, C_{fm}^* vs Ri for three values of H^* at $Re = 30$.

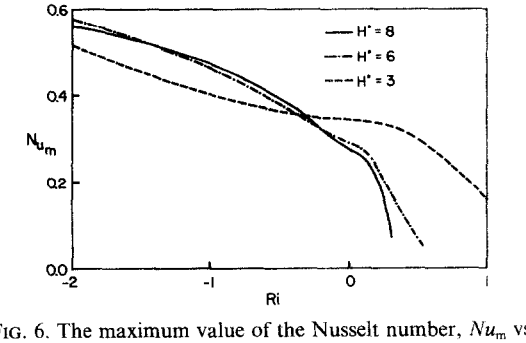

FIG. 6. The maximum value of the Nusselt number, Nu_m vs Ri for three values of H^* at $Re = 30$.

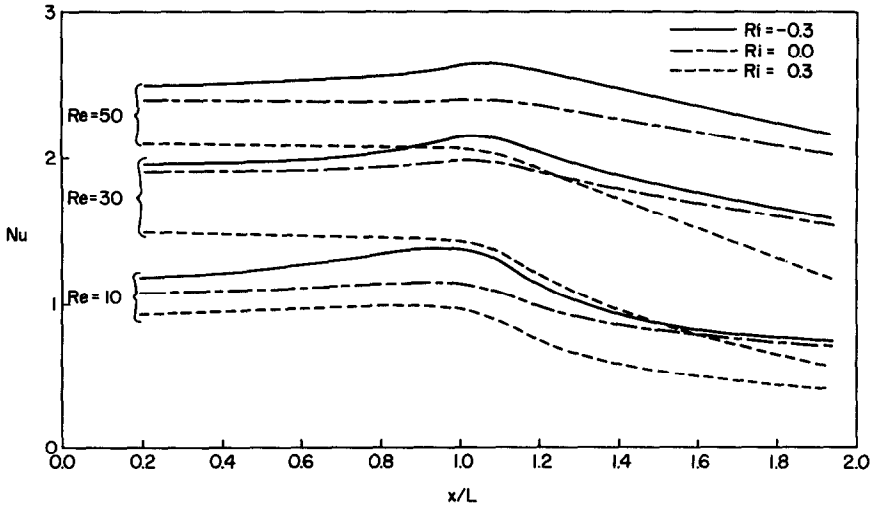

FIG. 7. Near impingement distribution of Nu for various values of Re and Ri, $H^* = 3$.

assisted and buoyancy retarded flows are presented. It is apparent that small increases in Re largely dominate the Richardson number effect in increasing Nu. However, there is a significant reduction of Nu when Ri becomes positive (opposing buoyancy). The increase of Nu for the same degree of assisting buoyancy is not as large. This conclusion is best illustrated by comparing the cases of $Re = 50$ and 30. The increase of Nu over the entire surface when Ri is decreased from 0 to -0.3 is significantly smaller than the decrease of Nu when Ri is increased to 0.3.

There is an apparent enhancement of the local Nusselt number near $x/l = 1$ for low Re and negative values of Ri. As Ri becomes more negative there is a predominant peak of Nu near $x/l = 1$. It is suggested that this rise of Nu is caused by the reduced spreading of the jet for assisted buoyancy which can be seen comparing the flow patterns in Figs. 2(a) with (c). The ability of the buoyancy forces to cause a noticeable peak near $x/l = 1$ is reduced as H^* increases. Figure 8 shows the near impingement Nusselt numbers for $H^* = 3$ and 6 for two values of Re. There is a near uniform reduction of Nu for $Re = 50$ when H^* is increased from 3 to 6. However, it is interesting that for $Re = 30$ only the region near $x/l = 1$ experiences a reduction of Nu when H^* is increased.

We have shown that including buoyancy effects in relatively short impingement distance flows there is a distinct impact on the local heat transfer coefficient distribution. As evidenced by Fig. 7 the effects of Re

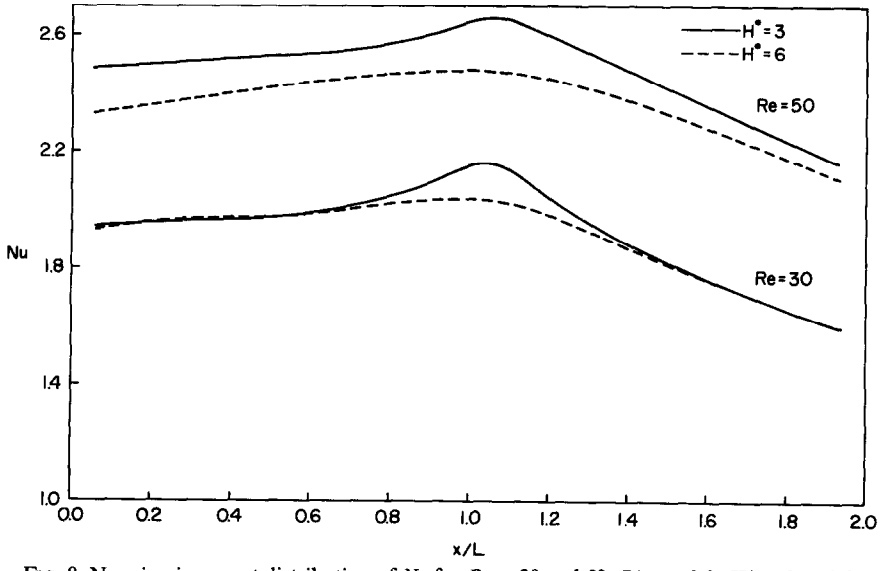

FIG. 8. Near impingement distribution of Nu for $Re = 30$ and 50, $Ri = -0.3$, $H^* = 3$ and 6.

and Ri are such that no generalized expression could be obtained for the Nu distribution which would collapse the results into a single functional form.

CONCLUSION

Results of the numerical predictions for upward and downward facing two-dimensional plane heated jets are presented. It can be concluded that the buoyancy effects on the magnitude of both C_f and Nu are significant and depend on the separation distance between the jet exit and the impinging surface. Flow separation along the impinging wall will occur in the downward facing flow for large Richardson numbers depending on H^*. For very large Richardson numbers the flow does not penetrate to the wall and the flow along the wall is a result of induced entrainment. Buoyancy alters the heat transfer coefficient distribution near impingement most notably by causing a distinct peak near $x/l = 1$. The reason for the enhanced surface heat transfer may be due to a reduction of jet spreading by the assisting buoyancy.

REFERENCES

1. F. E. Enrich, Some hydrodynamic aspects of valves, ASME paper 55-A-114 (1955).
2. H. Miyazaki and E. Silberman, Flow and heat transfer on a flat plate normal to a two-dimensional laminar jet issuing from a nozzle of finite height, *Int. J. Heat Mass Transfer* **15**, 2097–2107 (1972).
3. E. M. Sparrow and L. Lee, Analysis of flow field and impingement heat mass transfer due to a nonuniform slot jet, *Trans. ASME*, Series C, *J. Heat Transfer* **97**(2), 191–197 (1975).
4. R. Gardon and J. C. Akfirat, Heat transfer characteristics of impinging two-dimensional air jets, *Trans. ASME*, Series C, *J. Heat Transfer* **88**(1), 101–108 (1966).
5. E. M. Sparrow and T. C. Wong, Impingement transfer coefficients due to initially laminar slot jets, *Int. J. Heat Mass Transfer* **18**, 597–605 (1975).
6. M. Wolfshtein, Convection processes in turbulent impinging jet, Ph.D. Dissertation, London University (1968).
7. A. R. P. van Heiningen, A. S. Mujumdar and W. J. M. Douglas, Numerical prediction of the flow field and impingement heat transfer caused by laminar slot jet, *J. Heat Transfer* **98**, 654–658 (1976).
8. A. S. Mujumdar, Y. K. Li and W. J. M. Douglas, Evaporation under an impinging jet: a numerical model, *Can. J. Chem. Engng* **58**, 448–453 (1980).
9. S. Mikhail, S. M. Morcos, M. M. M. Abul-Ellail and W. S. Ghaly, Numerical prediction of flow field and heat transfer from a row of laminar slot jets impinging on a flat plate, *Proc. Seventh Int. Heat Transfer Conf.*, Vol. 3, pp. 337–382 (1982).
10. S. Satyanarayana and Y. Jaluria, A study of laminar buoyant jets discharged at an inclination to the vertical buoyancy force, *Int. J. Heat Mass Transfer* **25**, 1569–1577 (1982).
11. T. S. Chen, E. M. Sparrow and A. Mucoglu, Mixed convection in boundary layer flow on a horizontal plate, *J. Heat Transfer* **99**, 66–71 (1977).
12. Y. Mori, Buoyancy effects in forced laminar convection flow over a horizontal flat plate, *J. Heat Transfer* **83**, 479–482 (1961).
13. S. V. Patankar, *Numerical Heat Transfer and Fluid Flow*. Hemisphere, Washington, DC (1980).
14. J. P. van Doormaal and G. D. Raithby, Enhancement of the simple method for predicting incompressible fluid flows, *Numer. Heat Transfer* **7**, 147–163 (1984).
15. L. Howarth, On the calculation of the steady flow in the boundary layer near the surface of a cylinder in a stream, ARC RM 1632 (1935).
16. J. W. Gauntner, J. N. B. Livingood and P. Hrycak, Survey of literature on flow characteristics of a single turbulent jet impinging on a flat plate, NASA TN D-5652 (1970).
17. K. J. McNaughton and C. G. Sinclair, Submerged jets in short cylindrical vessels, *J. Fluid Mech.* **23**(2), 367–375 (1966).

EFFET DE FLOTTEMENT SUR DES JETS LAMINAIRES IMPACTANTS

Résumé—On étudie un jet laminaire, chaud, bidimensionnel qui frappe une surface isotherme, pour déterminer les effets de flottement sur la structure d'écoulement près de la région de l'impact. Les paramètres utilisés sont le nombre de Reynolds à la sortie du jet, le nombre de Richardson et la distance qui sépare la sortie du jet de la cible. Des résultats de profil de vitesse, de distribution de température, de coefficient de frottement et de transfert thermique sont présentés, à la fois pour des jets faisant face vers le haut ou vers le bas. On trouve que le nombre de Nusselt local montre un pic écarté de l'axe du jet et qui augmente pour des écoulements fortement flottants. En général, l'accroissement du flux thermique est substantiel pour des conditions de nombre de Richardson élevé.

AUFTRIEBSEFFEKTE IN EINEM LAMINAREN, AUF EINE WAND AUFTREFFENDEN STRAHL

Zusammenfassung—In einem laminaren, beheizten, zweidimensionalen Strahl, der auf eine isotherme Fläche auftrifft, wurde der Einfluß des Auftriebs auf Strömung und Temperaturverteilung nahe der Auftreffstelle untersucht. Die verwendeten Parameter sind: die Reynolds-Zahl am Strahlaustritt, die Richardson-Zahl und der Abstand zwischen Strahlaustritt und Aufprallfläche. Die Ergebnisse zeigen Geschwindigkeitsprofile, Temperaturverteilungen, örtliche Reibungsbeiwerte und Wärmeübergangskoeffizienten für senkrecht nach oben und unten gerichtete Strahlen. Es zeigt sich, daß die örtliche Nusselt-Zahl außerhalb der Strahlachse eine Spitze aufweist, die sich für einen Strahl mit einem straken Auftrieb erhöht. Ganz allgemein ergibt sich bei hohen Richardson-Zahlen eine spürbare Verbesserung des Wärmeübergangs.

ВЛИЯНИЕ СИЛ ПЛАВУЧЕСТИ НА ЛАМИНАРНЫЕ ИМПАКТНЫЕ СТРУИ

Аннотация—Для выяснения влияния сил плавучести на поля скорости и температуры в области соударения струи с преградой исследуется ламинарная нагретая двумерная струя, натекающая на изотермическую поверхность. Определяющими параметрами являются числа Рейнольдса и Ричардсона для струи на выходе из насадка, а также расстояние между поверхностью и срезом сопла. Результаты для профилей скорости и температуры, локального коэффициента трения и коэффициента теплообмена получены для струй, направленных вертикально вверх и вертикально вниз. Найдено, что локальное число Нуссельта достигает максимального значения на некотором расстоянии от оси струи и что это значение увеличивается с ростом эффекта плавучести. В общем отмечается значительная интенсификация теплопереноса при больших значениях числа Ричардсона.